

Decision-Aware Evaluation of Physics-Informed Surrogates

Daniel Cieślak^{1,*} and Andrzej Czyżewski¹

¹Gdańsk University of Technology, Gdańsk, Poland

*Corresponding author: daniel.cieslak@pg.edu.pl

ABSTRACT

Physics-informed machine learning is often assessed by curve error, although engineering use depends on downstream decisions: ranking candidates, avoiding infeasible designs and limiting regret. We introduce *pinn-gym*, an open benchmark for material-conditioned lattice design that couples a transparent reduced-order crush-and-impact oracle with five printable polymer cards, dimensionless force-response targets and a protocol spanning curve fidelity, physical admissibility, top- k retrieval and mass regret.

Across per-material, pooled and cross-material settings, low nRMSE is frequently insufficient to identify useful design selections. Physics-informed losses alter trade-offs rather than monotonically improving all metrics, and dimensionless conditioning improves comparability without making transfer symmetric. The benchmark is not a certified material model; within the released oracle, candidate generator and material cards, *pinn-gym* provides a reproducible testbed for evaluating PIML surrogates as decision systems rather than curve predictors alone.

Introduction

Physics-informed machine learning (PIML) is increasingly used to accelerate simulation and engineering design^{1–5}. Its promise is not only better interpolation, but more reliable decisions under physical constraints. In design workflows, however, the surrogate is rarely the final object of interest. It ranks candidate geometries, rejects infeasible designs and guides expensive downstream simulation or fabrication. A model can therefore be accurate as a force–displacement predictor while still being a poor design assistant.

We introduce *pinn-gym*, an open benchmark for decision-aware evaluation of material-conditioned PIML surrogates in lattice energy absorption. The benchmark defines a transparent reduced-order oracle, five printable polymer material cards, candidate pools, baseline models, physics-informed losses and metrics that jointly report curve fidelity, physical admissibility, top- k retrieval and mass regret. The target domain is deliberately narrow enough to be reproducible and broad enough to stress material conditioning: the same geometry can behave differently under compliant TPU and stiff carbon-fibre-reinforced PA cards^{6–11}.

The central modelling choice is nondimensionalisation. Following scaling-law modelling and Buckingham- π analysis^{13,14}, the surrogate predicts a dimensionless force response

$$\hat{f}(\boldsymbol{\varepsilon}; g^*, m^*) = \frac{F}{\sigma_y A_{\text{env}}}, \quad \boldsymbol{\varepsilon} = \frac{u}{L_{\text{env}}}, \quad (1)$$

conditioned on nondimensional geometry g^* and a material vector m^* encoding stiffness, strength, plateau response, failure strain, density, printability and rate-sensitivity ratios. Changing the polymer is therefore an input perturbation rather than a separate regression task. This supports three evaluations: per-material specialists, one pooled material-conditioned model and zero-shot cross-material transfer.

This framing separates three questions that are often conflated. First, does low held-out curve error imply useful design ranking? Second, do physics-informed losses improve the downstream decision or merely shift the trade-off between fit and constraint satisfaction? Third, does dimensionless material conditioning make transfer symmetric across polymer regimes? The answer to all three is non-trivial. Across the released benchmark, lower nRMSE often fails to identify the best feasible designs, additional residual terms are not uniformly beneficial, and transfer remains asymmetric despite dimensionless inputs.

The contribution is therefore a benchmark and protocol, not a certified absorber. All claims are scoped to the declared oracle, candidate generator and material cards. The purpose is to make PIML evaluation closer to how surrogates are actually used: as decision systems whose curve predictions matter only insofar as they produce feasible, low-regret choices.

pinn-gym: a decision-aware benchmark for physics-informed surrogates

From candidates and a declared oracle to design utility: evaluate what matters, not just curve error.

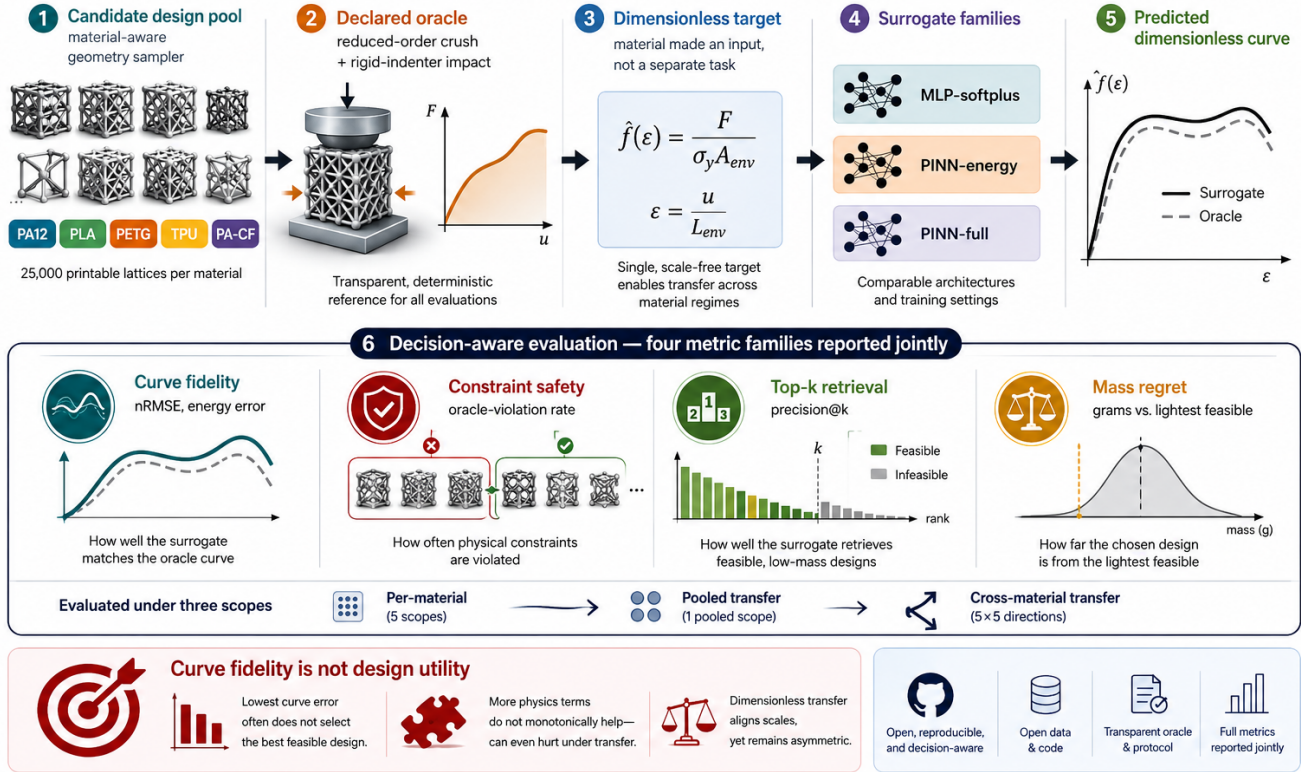


Figure 1. Overview of the *pinn-gym* benchmark. A material-aware sampler draws candidate lattice geometries for five printable polymer cards; a declared reduced-order crush-and-impact oracle labels every candidate with a force–displacement curve, absorbed energy, peak force and a feasibility outcome. Force and displacement are nondimensionalised to the target $\hat{f}(\epsilon) = F / (\sigma_y A_{env})$, which makes the polymer an input rather than a separate regression task. Three surrogate families (data-only MLP-softplus, energy-informed PINN, composite PINN) are trained and then evaluated under three scopes (per-material, pooled, 5×5 transfer) through four metric families reported jointly: curve fidelity, constraint safety, top- k retrieval and mass regret. The central result of the benchmark is that these families do not agree: the surrogate with the lowest curve error is frequently not the one that selects the best feasible design.

Results

What the benchmark measures, and how the study is organised

pinn-gym is a controlled diagnostic environment, not a material-property claim. The oracle is transparent, deterministic and shared across all models, so differences between methods reflect surrogate behaviour under the same labelling rule. A higher-fidelity FEM or experimental oracle would change the absolute numbers, but not the need to evaluate prediction, constraint satisfaction and selection jointly.

The study has a simple structure (Table 1). We first describe the task and the feasible-set structure induced by five material cards. We then compare per-material specialists, pooled material-conditioned models and 5×5 zero-shot transfers. The reported metrics are deliberately heterogeneous: curve nRMSE measures interpolation, violation rate measures safety under the oracle, precision-at- k measures retrieval of feasible designs, and regret-at- k measures the mass penalty of the selected design. No single metric is treated as sufficient.

pinn-gym defines a material-conditioned decision benchmark

The benchmark holds out oracle-labelled candidate pools for five material cards and evaluates all surrogates on identical inputs. A material-aware sampler, described in Methods, centres each pool around the declared peak-force frontier so that easy and

Table 1. Study structure and the role of each experiment block.

Block	Purpose
Task definition	Defines the oracle-labelled material-conditioned candidate pools and feasible-set structure.
Per-material models	Tests whether curve fidelity predicts design ranking when each material has its own specialist.
Pooled models	Tests whether one dimensionless material-conditioned surrogate can replace specialists.
Transfer matrix	Tests whether a checkpoint trained on one material transfers symmetrically to another.
Seed repeats	Tests whether decision-aware conclusions survive stochastic retraining.

Table 2. Held-out evaluation pools by material card. Feasibility is assigned by the declared numerical oracle. Mass values are reported in grams.

Material	Candidates	Feasible	Feasible [%]	Median mass	Mass range
PA12	25,000	4,383	17.53	62.9	27.4–90.9
PLA	25,000	6,254	25.02	82.4	40.8–111.6
PETG	25,000	4,371	17.48	84.1	40.0–114.3
TPU	25,000	16,149	64.60	78.7	35.0–108.0
PA-CF	25,000	3,211	12.84	73.3	33.6–103.5

hard candidates coexist wherever the fixture constraints admit feasible designs. The fixture constraints are fixed across materials at a peak-force limit of 3500 N and a minimum crush distance of 40 mm under a 6 kg, 0.5 m drop (29.43 J). Differences in feasibility therefore come from the material card and candidate geometry, not from re-tuning the task per polymer.

The first benchmark result is descriptive but important: the same oracle creates very different design regimes across material cards (Table 2, Fig. 2). Compliant and stiff polymers occupy different regions of mass, peak force and crush distance even under the same geometric envelope. This matters for PIML evaluation because a single curve-error number does not reveal whether a target pool contains many feasible low-mass designs, very few feasible designs or no feasible designs under the declared fixture. We therefore treat feasibility priors as part of the benchmark, not as incidental dataset statistics.

Lower curve error does not imply better design rankings

The clearest evidence for reporting multiple metric families is that, on a single card, curve accuracy and design ranking can disagree (Table 3, Fig. 3). On PLA, the energy-informed PINN attains the lowest curve error in the main protocol (nRMSE 0.119), but the data-only MLP retrieves more oracle-feasible candidates in the top-10 screening set despite a higher curve error (nRMSE 0.462). Because $P@10$ is a deliberately small-budget screening metric, these values should be read as evidence of metric disagreement rather than as a precise estimate of a stable performance ratio. On PA-CF the reversal is sharper: the lowest-curve-error model (MLP, nRMSE 0.260) endorses unsafe designs at a 0.40 oracle-violation rate and reaches only $P@10 = 0.2$, whereas the higher-error energy PINN (nRMSE 0.402) is constraint-safe and retrieves every feasible design in its top ten ($P@10 = 1.0$). A curve-error leaderboard would therefore miss decision-relevant failures that become visible only when curve fidelity, feasibility and retrieval are reported jointly.

This is the central scientific message of the benchmark. For design, the relevant question is not simply whether the surrogate predicts $F(u)$ accurately, but whether its prediction induces a useful ordering over candidate geometries. Precision-at- k and regret-at- k expose this ordering. We use $P@10$ as an interpretable small-budget screening metric, not as a continuous estimator of ranking quality; broader values of k are included in the evaluation harness to check whether the same disagreement persists beyond the top-ten budget. Regret is especially useful because it converts ranking quality into an engineering quantity: the mass penalty paid relative to the lightest oracle-feasible candidate available in the pool. When the feasible set is empty under the declared fixture, ranking metrics are reported as non-applicable rather than as failures. This distinction is essential for stiff cards and prevents the benchmark from confusing sampler and constraint geometry with model quality.

Physics-informed losses change the trade-off, not just the fit

The energy-informed model and the composite PINN should not be read as a monotonic ladder in which more residual terms automatically imply a better surrogate. The energy residual often acts as a useful prior over the feasible region: it shapes the predicted curve in a way that can reduce physically inadmissible selections and improve energy consistency. The additional peak-force, monotonicity-after-densification and smoothness penalties are individually defensible, but their scalarised combination changes the optimisation landscape. In several settings the composite objective improves one quantity while

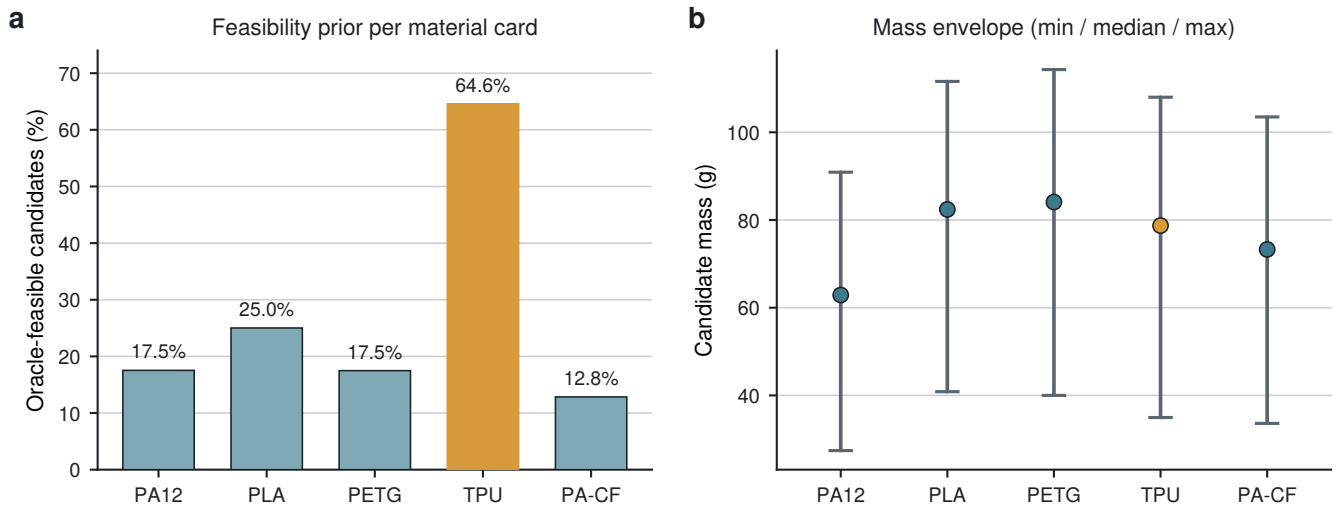


Figure 2. One oracle, five design regimes. (a) Fraction of oracle-feasible candidates in each held-out pool under the fixed fixture; the compliant TPU card (highlighted) is feasible for 64.6% of candidates, whereas the stiff PA-CF card is feasible for only 12.8%. (b) The corresponding candidate-mass envelope (minimum, median and maximum) shows that the cards also occupy different regions of the mass axis. Because feasibility differs by a factor of five across cards, feasibility priors are treated as part of the benchmark rather than as incidental dataset statistics; they set the ceiling on what any surrogate can retrieve.

weakening another.

This behaviour is not a reason to discard physics-informed learning. It is the reason to benchmark it decision-wise. In *pinngym*, the correct question is not “does the constraint help?” but “which part of the design objective does the constraint help?” A residual can improve energy-integral behaviour, reduce violation rate or regularise extrapolation without being the model with the lowest nRMSE. The loss-weight ablation in Table 4 makes this dependence explicit. A boundary-only objective collapses to high predicted-feasible rates and poor curve fit, while energy and composite objectives reduce curve error by an order of magnitude. Strengthening different physics terms changes the trade-off surface: the peak-strong setting gives the lowest macro nRMSE in this ablation (0.219) and zero mean violation, whereas the default composite gives slightly higher nRMSE (0.250) but a different feasible-retrieval profile. This is exactly the behaviour the benchmark is designed to expose.

Pooled material conditioning fits curves but does not unify decisions

The pooled setting tests whether one nondimensional, material-conditioned surrogate can replace five specialists. On the main held-out pools, a single pooled network learns the material conditioning and reaches moderate curve error on every card, with nRMSE between 0.38 and 0.69. However, the decision metrics remain target-specific. On TPU, the composite PINN reaches $P@10 = 0.9$, whereas the energy-informed PINN trained on the same pooled data retrieves no oracle-feasible design in its top ten ($P@10 = 0$). On PETG and PA-CF, some pooled variants select predicted-feasible candidates that the oracle rejects entirely, giving violation rates of 1.0. Thus pooled curve accuracy is necessary but not sufficient: one model can fit all five material cards while still making poor design selections on individual targets. The per-card numbers are reported in Table 6 and Fig. 4.

We repeated the pooled experiment after correcting pooled step scaling and tuning capacity. This second protocol confirms the same message in a less pessimistic setting: tuned pooled models can reach competitive curve errors and sometimes strong decision performance, but the best trade-off is still material-dependent. In the capacity ablation, increasing width and depth improves curve accuracy, whereas decision metrics saturate or move non-monotonically. In the loss-weight ablation, energy, peak-force and composite terms improve different parts of the objective rather than forming a universal ordering.

The practical conclusion is not that pooled conditioning fails. It is that pooled PIML must be evaluated per target material and per downstream use. For early screening, a slightly less accurate model with lower violation rate may be preferable. For curve interpolation, the opposite may hold. Reporting only a pooled average nRMSE would hide this distinction.

Dimensionless transfer aligns scales but stays asymmetric

The 5×5 transfer matrix asks a different question from pooled training. Each off-diagonal entry is produced by taking a checkpoint trained on one material, re-scaling its inputs with the target material’s nondimensional groups and evaluating it on the target pool without retraining or fine-tuning (Fig. 5). If nondimensionalisation removed all material-regime bias, the matrix would be close to symmetric. It is not. The clearest case is the PA12–TPU pair: a TPU-trained checkpoint transfers

Table 3. Material-specific surrogate evaluation (main protocol). Specialists trained and evaluated on a single card, on the 25,000-candidate held-out pools; rows are ordered by curve error within each card to make the accuracy–utility dissociation visible. Lower nRMSE, violation and regret are better; higher P@10 is better. ∞ marks a non-empty feasible pool from which the model retrieved no feasible design in its top ten.

Material	Method	nRMSE ↓	Violation ↓	P@10 ↑	Regret@10 [g] ↓
PA12	PINN-energy	0.184	0.000	1.000	0.28
PA12	MLP-softplus	0.596	0.000	1.000	1.03
PA12	PINN-full	0.704	0.000	1.000	0.57
PLA	PINN-energy	0.119	0.000	0.200	5.00
PLA	PINN-full	0.408	0.000	0.000	∞
PLA	MLP-softplus	0.462	0.000	0.500	5.82
PETG	PINN-energy	0.405	0.000	1.000	5.92
PETG	PINN-full	0.408	0.000	0.700	5.92
PETG	MLP-softplus	0.408	0.000	0.000	∞
TPU	PINN-energy	0.252	0.104	0.000	∞
TPU	MLP-softplus	0.670	0.000	0.000	∞
TPU	PINN-full	0.694	0.000	0.000	∞
PA-CF	MLP-softplus	0.260	0.399	0.200	0.00
PA-CF	PINN-energy	0.402	0.000	1.000	6.89
PA-CF	PINN-full	0.410	0.000	0.100	0.00

Table 4. Physics-loss weight ablation (revision protocol). Effect of the physics-loss weights on pooled `pinn_full`. Values are macro-averaged over the five material cards; `regret@10` is averaged only over cards on which a finite regret is defined. Lower nRMSE, energy error, violation and regret are better; higher P@10 is better. The default composite row uses the declared weights of Table 5. Because this ablation is run on the re-sampled revision pools, its absolute numbers are a within-protocol sensitivity analysis and are not directly comparable to the main 25,000-candidate pools.

Ablation	Loss weights					Macro-averaged metrics					
	w_b	w_E	w_p	w_m	w_s	nRMSE ↓	Energy err. [J] ↓	Violation ↓	Pred.-feas.	P@10 ↑	Regret@10 [g] ↓
Boundary only	0.05	0	0	0	0	1.645	35.496	0.692	0.800	0.060	2.691
Energy only	0.05	0.20	0	0	0	0.286	10.431	0.440	0.007	0.300	2.180
Default composite	0.05	0.20	0.10	0.05	0.02	0.250	10.078	0.636	0.007	0.320	2.180
Energy-strong	0.05	0.50	0.10	0.05	0.02	0.272	13.708	0.200	0.001	0.380	1.939
Peak-strong	0.05	0.20	0.30	0.05	0.02	0.219	9.733	0.000	0.000	0.380	1.939

onto the PA12 pool with curve error nRMSE = 0.32 and recovers the entire feasible top-10 ($P@10 = 1.0$), whereas the reverse direction, PA12 onto TPU, degrades to nRMSE = 11.3 and retrieves nothing ($P@10 = 0$)—a more than thirty-fold gap in curve error between two directions that the dimensionless formulation makes nominally equivalent. The asymmetry is not confined to that pair: the PLA–PA12 direction shows the same ordering on a smaller scale (0.27 versus 0.68), and several transfers preserve acceptable curve error while still retrieving no feasible top-ranked candidate. Transfers from compliant regimes onto stiffer ones are systematically easier than the reverse.

This result should be read constructively. The transfer matrix is a diagnostic for future PIML methods rather than a statement that transfer is impossible. It identifies where a single-material checkpoint has learned response-shape statistics that do not extrapolate across material groups, and it separates three kinds of transfer success: curve prediction, feasible retrieval and constraint safety. A new surrogate, neural operator or meta-learning method can be evaluated against exactly the same matrix and can claim improvement only when it reduces this asymmetry in the relevant metric family rather than in one curve number.

Repeated seeds support the benchmark message

To reduce the risk that the conclusions are single-run artefacts, the revision experiments repeat the PINN-energy and PINN-full variants over five seeds and summarise mean and standard deviation per card (Table 7). These repeats are used to test the qualitative benchmark message, not to turn the single-seed main protocol into a definitive ranking of model families. The repeated runs preserve the main conclusion that physics-informed losses alter the balance between curve error, predicted

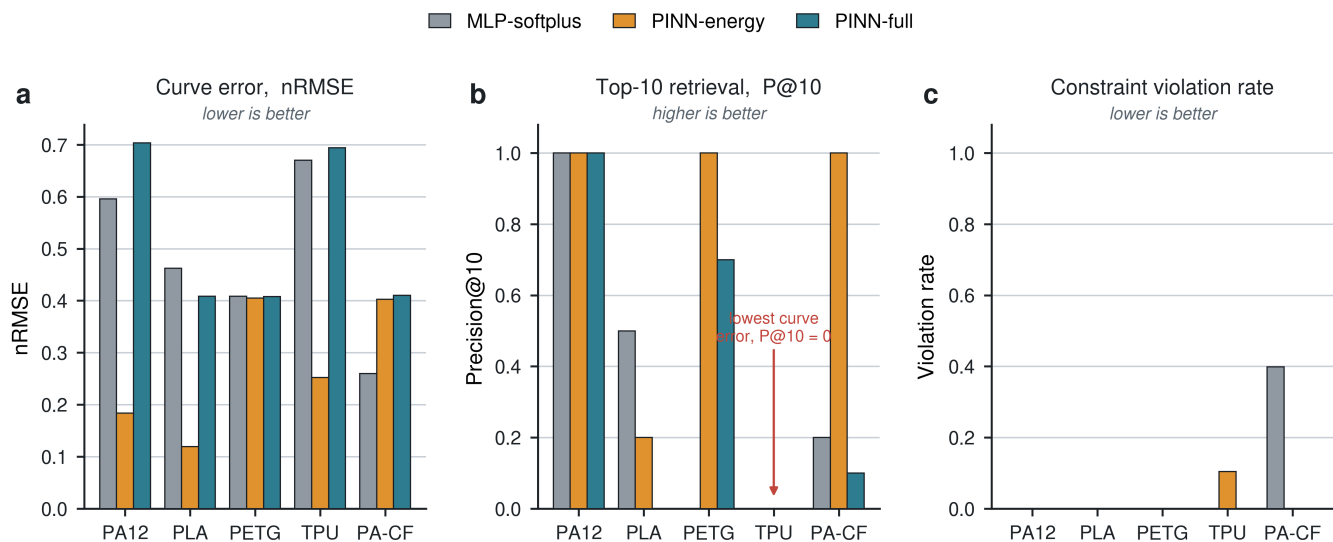


Figure 3. Curve accuracy and design utility disagree within a single material card. Per-material surrogate metrics for the three model families across (a) curve fidelity (nRMSE, lower is better), (b) top-10 feasible retrieval (P@10, higher is better) and (c) oracle-violation rate (lower is better). The highlighted case marks a card on which the lowest-curve-error model retrieves no feasible design in its top ten. Read together with Table 3, the panels show that the best curve predictor is frequently neither the safest nor the most useful ranker.

Table 5. Declared default physics-loss weights used for the composite PINN. The weights are treated as benchmark choices and ablated rather than as universal constants.

Loss term	Weight
Boundary consistency	0.05
Energy residual	0.20
Peak-force penalty	0.10
Post-densification monotonicity	0.05
Curvature smoothness	0.02

feasibility, violation rate and regret, and that these outputs cannot be inferred from nRMSE alone. They also show why decision metrics should be reported with uncertainty: for TPU, PINN-full has a high nRMSE standard deviation (0.339) and a predicted-feasible-rate standard deviation of 0.422, whereas other cards are more stable.

Discussion

pinn-gym makes physics-informed learning measurable at the point where it matters for engineering design: candidate selection. The benchmark does not ask only whether a surrogate predicts a force–displacement curve. It asks whether that prediction leads to physically admissible, low-mass and high-value choices under a declared oracle.

Decision-aware evaluation is the main contribution. Curve fidelity, physical admissibility and design utility are not interchangeable. In the benchmark, a surrogate can improve nRMSE while worsening top- k retrieval, or reduce oracle violations while sacrificing pointwise fit. This is expected when a regression model is used as a ranking function. Engineering PIML papers should therefore report prediction metrics, physical metrics and decision metrics together.

Physics-informed losses are design priors. The energy residual is useful because it shapes the feasible decision boundary, not because it universally minimises every error measure. Additional peak-force, monotonicity and smoothness penalties are physically reasonable, but scalarising several residuals can move the optimiser away from the best trade-off for a given design workflow^{18–22}. The practical recommendation is to add physics terms one at a time, declare their weights and report effects on curve error, violation rate and regret.

Dimensionless conditioning helps but does not solve transfer. The pooled experiments show the positive result: one nondimensional, material-conditioned network can cover several polymer cards. The transfer matrix gives the caution: changing

Table 6. Pooled material-conditioned surrogate evaluation (main protocol). A single network is trained across all five cards and evaluated per card on the 25,000-candidate held-out pools; these are the numbers visualised in Fig. 4. A pooled model can reach moderate curve error on every card while its decision metrics remain strongly card-specific. Lower nRMSE, violation and regret are better; higher P@10 is better.

Material	Method	nRMSE ↓	Violation ↓	P@10 ↑	Regret@10 [g] ↓
PA12	MLP-softplus	0.597	0.000	1.000	0.00
PA12	PINN-energy	0.551	0.000	0.900	1.68
PA12	PINN-full	0.594	0.000	0.500	16.07
PLA	MLP-softplus	0.408	0.000	0.000	∞
PLA	PINN-energy	0.386	0.000	0.700	8.31
PLA	PINN-full	0.407	0.000	0.000	∞
PETG	MLP-softplus	0.409	0.000	0.000	∞
PETG	PINN-energy	0.388	0.000	0.000	∞
PETG	PINN-full	0.408	1.000	0.100	26.07
TPU	MLP-softplus	0.694	0.000	0.000	∞
TPU	PINN-energy	0.623	0.000	0.000	∞
TPU	PINN-full	0.690	0.000	0.900	12.71
PA-CF	MLP-softplus	0.410	0.000	0.200	0.00
PA-CF	PINN-energy	0.383	1.000	0.000	∞
PA-CF	PINN-full	0.409	0.000	0.200	14.83

Columns. nRMSE: curve fidelity (lower is better); Violation: fraction of predicted-feasible candidates the oracle rejects; P@10: top-10 feasible-retrieval precision; Regret@10: mass gap in grams to the lightest oracle-feasible design. *Symbols.* ∞ marks a non-empty feasible pool from which the model retrieved no feasible candidate in its top ten (a decision failure, not a missing pool); N/A would mark a pool with no oracle-feasible candidate, which does not occur in the main 25,000-candidate pools. All rows use the main protocol.

material cards is not a symmetric perturbation. A checkpoint trained in one regime can carry response-shape biases that fail in another. This makes transfer matrices a useful diagnostic for neural operators, uncertainty-aware surrogates and active-learning policies, not merely for the baselines used here.

The benchmark is intentionally oracle-scoped. The released oracle is not a substitute for FEM or experiment. Its value is that it is transparent, cheap and fixed, which makes it useful for method comparison. A future high-fidelity version could replace the oracle while preserving the same protocol: evaluate curve prediction, physical admissibility, retrieval and regret jointly. Whenever aggregate regret is reported, it is computed only over finite selected designs and should be interpreted together with the corresponding retrieval-failure rate. Infinite regret is therefore a categorical decision failure in the tables, not a numeric value averaged with finite masses.

Limitations

The benchmark is oracle-scoped by design. The five material cards encode declared assumptions about density, stiffness, yield, plateau response, failure strain, printable feature limits and strain-rate sensitivity. They are not calibrated to a specific filament batch, printer, build orientation or post-processing condition. The reduced-order crush model and rigid-indenter impact integration provide a transparent labelling rule rather than certified finite-element predictions. The fixture limits (peak force 3500 N, crush distance 40 mm and 29.43 J impact energy) define the benchmark task, not an experimentally certified safety margin.

The ranking metrics must also be interpreted with the feasible set in mind, and the tables separate two cases that are easy to conflate. When the declared candidate pool for a material contains no oracle-feasible design under the fixed fixture, precision-at- k and regret-at- k are non-applicable (denoted N/A) rather than evidence that a model failed to select a feasible design. When a feasible set exists but a model retrieves none of its members in the top- k , regret is infinite (denoted ∞). These cases are kept distinct in every table because conflating them would overstate model failure and understate the role of candidate-pool geometry.

Finally, the pooled-tuning results are intended as a sensitivity analysis of the benchmark and modelling pathway, not as a claim that the selected architecture is globally optimal. The benchmark should therefore be read as a controlled, reproducible environment for comparing PIML design surrogates under a declared oracle. It is complementary to, not a substitute for, high-fidelity FEM and physical testing campaigns required before any lattice absorber can be deployed.

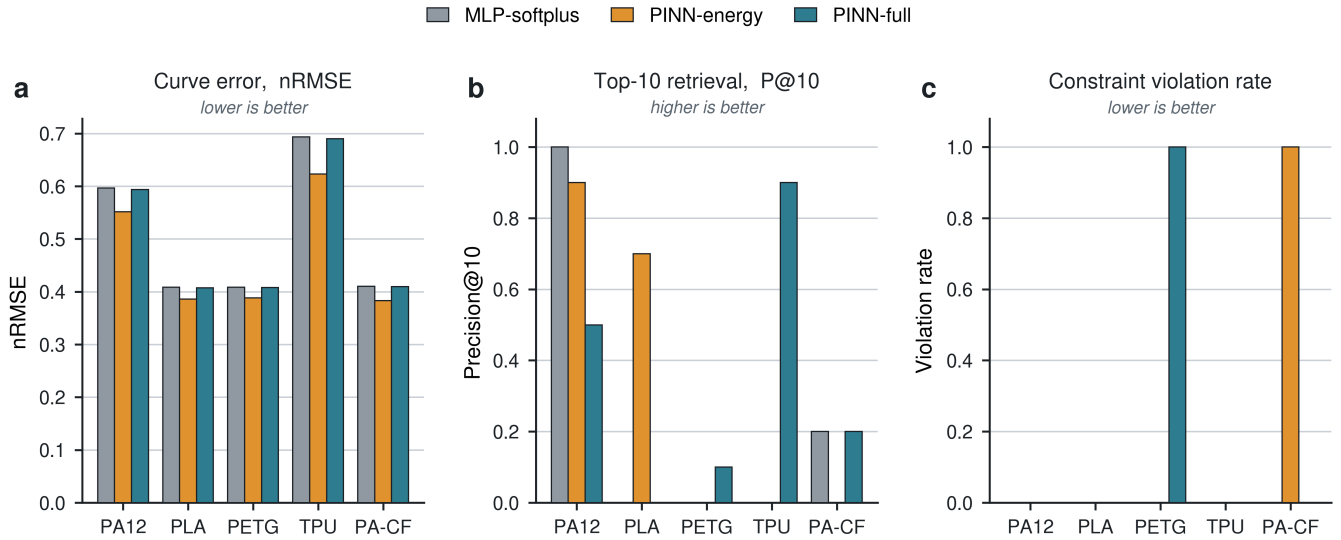


Figure 4. Pooled material-conditioned evaluation. A single nondimensional surrogate can fit multiple material cards, but curve error, oracle violations and top- k retrieval remain partially decoupled.

Table 7. Five-seed repeat summary from the revision experiments. Values are mean \pm standard deviation by material and method. Regret@10 is reported according to the revision protocol and is finite only where a feasible selected design exists.

Material	Method	nRMSE	Pred.-feas.	Violation	Regret@10 [g]
PA12	PINN-energy	0.196 \pm 0.065	0.001 \pm 0.001	0.000 \pm 0.000	0.000 \pm 0.000
PA12	PINN-full	0.388 \pm 0.174	0.011 \pm 0.024	0.034 \pm 0.076	0.000 \pm 0.000
PA-CF	PINN-energy	0.108 \pm 0.016	0.000 \pm 0.000	0.000 \pm 0.000	0.453 \pm 0.754
PA-CF	PINN-full	0.241 \pm 0.152	0.008 \pm 0.017	0.027 \pm 0.060	0.755 \pm 1.557
PETG	PINN-energy	0.111 \pm 0.010	0.000 \pm 0.000	0.200 \pm 0.447	1.751 \pm 2.643
PETG	PINN-full	0.202 \pm 0.094	0.006 \pm 0.014	0.097 \pm 0.218	0.574 \pm 1.230
PLA	PINN-energy	0.094 \pm 0.010	0.000 \pm 0.000	0.000 \pm 0.000	0.582 \pm 0.797
PLA	PINN-full	0.205 \pm 0.124	0.008 \pm 0.018	0.204 \pm 0.445	0.290 \pm 0.648
TPU	PINN-energy	0.195 \pm 0.061	0.001 \pm 0.001	0.000 \pm 0.000	11.663 \pm 3.323
TPU	PINN-full	0.413 \pm 0.339	0.444 \pm 0.422	0.145 \pm 0.178	5.609 \pm 4.708

Methods

The benchmark, surrogate code, oracle definition, candidate pools, training scripts and evaluation harness are available through the project repository at <https://github.com/Dyniel/pinn-gym>. Run metadata for every reported number, including the random seed or seed list, checkpoint hashes and candidate-pool generator state, is recorded in the per-run JSON files distributed with the archive so that every figure and table in the manuscript can be regenerated end to end.

Main and revision experiment protocols

The manuscript combines two compatible evaluation protocols. The main benchmark protocol uses the 25,000-candidate held-out pools per material to compare per-material specialists, pooled models and cross-material transfer under a single declared oracle. The revision protocol uses the same oracle, material cards, metrics and reporting conventions, but adds pooled-step-scaling correction, physics-loss weight ablation, pooled capacity tuning and five-seed repeats. We report these revision experiments separately when their candidate-pool geometry differs from the main 25,000-candidate pools; in particular, top- k retrieval and regret are treated as non-applicable when a revision pool has no oracle-feasible candidate under the fixed fixture. This separation prevents model failure from being conflated with absence of feasible designs in the candidate pool.

Declared numerical oracle

The declared oracle combines a reduced-order layered crush model with a rigid-indenter dynamic impact integrator. Each candidate is first mapped to geometric descriptors (cell size, wall and cap thicknesses, edge-rib geometry, envelope dimensions, derived relative density), and then to a predicted mass, a force-displacement curve $F(u)$, an absorbed-energy integral $E_{\text{abs}} =$

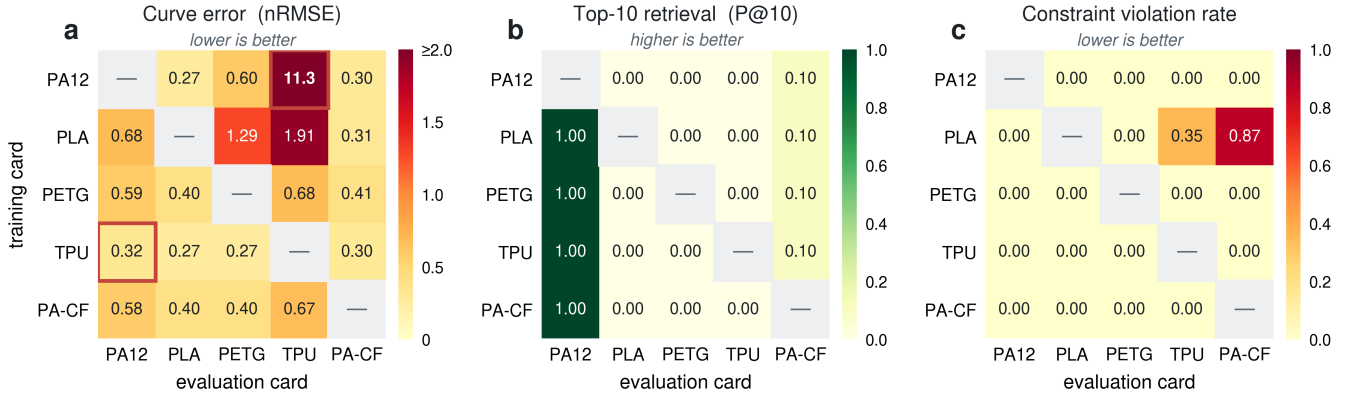


Figure 5. Dimensionless conditioning aligns scales but leaves cross-material transfer strongly asymmetric.

Cross-material transfer of the PINN-energy model across five material cards. Rows denote the material used for training and columns the material used for evaluation; diagonal entries are omitted because self-material performance is reported separately. Panel A shows curve-prediction error as nRMSE (highlighted cells mark the PA12–TPU pair, where the two directions differ by more than thirtyfold). Panel B reports top-10 retrieval precision for oracle-feasible candidates under the predicted design score. Panel C reports the fraction of predicted-feasible candidates that violate oracle constraints. Curve-level transfer and design-selection utility are not equivalent, and neither is symmetric across training and evaluation cards.

$\int F du$, a peak force, and an impact-survival outcome from a 6 kg, 0.5 m drop (29.43 J of incident kinetic energy). A candidate is labelled oracle-feasible when both the crush model and the impact integration satisfy the fixture limits $F_{\max} \leq 3500$ N and crush displacement ≥ 40 mm. The oracle is deterministic given the geometry and the material card; it is fully described in code and contains no machine-learned components, so it can be re-implemented or audited independently of any specific simulator. The fixture limits define the benchmark task, not an experimentally certified safety margin.

Material cards

Five material cards span the printable-polymer regime: PA12, PLA, PETG, TPU (thermoplastic polyurethane) and PA-CF (carbon-fibre-reinforced polyamide). Each card declares density, elastic modulus, yield strength, plateau-to-yield ratio, failure strain, z -direction anisotropy, printer tolerance, minimum printable feature size and a strain-rate sensitivity factor. The cards are numerical modelling inputs, not experimentally calibrated filament batches; full numerical values are tabulated in the repository so that researchers extending the benchmark can add new cards on the same footing.

Material-aware candidate sampling

For each card, the sampler centres the candidate pool on the declared peak-force frontier. The relative load-bearing area scale is

$$\phi_{\text{peak}} = \frac{F_{\text{lim}}}{\sigma_y A_{\text{env}}}, \quad (2)$$

with $F_{\text{lim}} = 3500$ N. The sampling band width is clamped to $[0.10, 0.22]$, and geometric bounds for walls, cells, caps, edge ribs and minimum features are adjusted using the card’s minimum printable feature size and printer tolerance. The intent is to produce per-card pools that straddle the feasibility frontier where one exists inside the printable-geometry envelope: rejection-only sampling would over-represent infeasible designs on PA-CF and under-represent the easy-feasible bulk on TPU.

Dimensionless scaling

For each material card, force, energy and displacement are nondimensionalised as

$$F_{\text{scale}} = \sigma_y A_{\text{env}}, \quad E_{\text{scale}} = F_{\text{scale}} \frac{L_{\text{env}}}{1000}, \quad \varepsilon = \frac{u}{L_{\text{env}}}, \quad \hat{f} = \frac{F}{F_{\text{scale}}}, \quad (3)$$

with σ_y in MPa and A_{env} in mm^2 (so 1 MPa = 1 N/ mm^2). The material descriptors are nondimensionalised against PA12 as a reference card. The 10-dimensional material vector m^* contains: stiffness ratio, yield ratio, plateau-to-yield ratio, failure-strain ratio, density ratio, minimum-feature ratio, tolerance ratio, z -anisotropy, strain-rate factor and yield-to-modulus ratio. This vector is the only material-specific input the network sees; the geometric descriptors g^* are themselves ratios (relative density, cell-to-envelope, wall-to-cell, etc.) and the strain ε is dimensionless by construction.

Surrogate architecture and training

The surrogate is a fully connected residual MLP with SiLU activations and a softplus output head that enforces non-negativity of \hat{f} . The input is the concatenation of the geometric descriptors g^* , the 10-dimensional material vector m^* and the strain ε . The output is the nondimensional force $\hat{f}(\varepsilon; g^*, m^*)$ evaluated on a fixed strain grid; the full $F(u)$ curve is reconstructed by multiplying by F_{scale} . The network has four residual blocks of width 256, layer normalisation and dropout disabled in the reported runs to keep the loss-term ablation interpretable. Three loss variants are trained from the same initialisation and the same data: **MLP-softplus** (data loss and a weak zero-displacement boundary penalty); **PINN-energy** (adds a dimensionless trapezoidal energy-integral residual); **PINN-full** (adds peak-force, post-densification monotonicity and curvature-smoothness terms).

The trained objective is

$$\mathcal{L} = \mathcal{L}_{\text{data}} + \lambda_b \mathcal{L}_{\text{boundary}} + \lambda_E \mathcal{L}_{\text{energy}} + \lambda_p \mathcal{L}_{\text{peak}} + \lambda_m \mathcal{L}_{\text{mono}} + \lambda_s \mathcal{L}_{\text{smooth}}, \quad (4)$$

with unused terms set to zero in each variant. The boundary term enforces $\hat{f}(0) = 0$. The energy term matches the dimensionless trapezoidal integral $\sum_i \hat{f}_i \Delta \varepsilon$ to the oracle absorbed energy divided by E_{scale} . The peak term penalises predicted forces above a soft bound expressed in \hat{f} . The monotonicity term penalises negative derivatives after the densification strain estimated from the predicted curve. The smoothness term penalises the second-order finite difference of \hat{f} along the strain grid. Optimisation uses Adam with an initial learning rate of 10^{-3} , cosine decay to 10^{-5} , batch size 512, 300 epochs per checkpoint and gradient clipping at ℓ_2 norm 1.0. The main-protocol runs use the fixed random seed 20260519; the revision repeat experiments use five seeds as reported in Table 7; per-material specialists are trained on 50,000 oracle-labelled candidates per card not included in the held-out pool, and the pooled model is trained on the union, with material card balancing per batch.

Evaluation metrics

Evaluation is performed on 25,000 oracle-labelled held-out candidates per material card. Metrics are stratified per card and reported jointly. Curve RMSE is in newtons, curve nRMSE divides by the per-card oracle force range, mean absolute energy-integral error is reported in joules. The decision-level metrics are: predicted-feasible rate (the fraction of candidates the surrogate would endorse as feasible at its internal threshold), physical-violation rate (the fraction of those endorsements rejected by the oracle), precision-at- k for $k \in \{1, 5, 10, 25, 50\}$ on the top-ranked predicted-feasible candidates ranked by mass, and regret-at- k defined as the mass gap between the lightest feasible candidate retrieved in the top- k and the lightest oracle-feasible candidate in the full pool. Regret is reported in grams. We use two distinct symbols for non-finite regret and apply them consistently in every table. N/A marks a material pool that contains *no* oracle-feasible candidate under the fixed fixture, so precision-at- k and regret-at- k are not applicable and must not be read as a model failure. ∞ marks the opposite case: the pool does contain oracle-feasible candidates, but the model retrieved none of them in its top- k , so the mass penalty relative to the lightest feasible design is unbounded—a genuine decision failure. All five main 25,000-candidate pools contain feasible candidates (Table 2), so ∞ in a main-protocol table always denotes a model failure; N/A arises only in the revision protocol, where re-sampling around the feasibility frontier can empty the feasible set for a card. Reference baselines are random ranking, lightest-first ranking, a pseudo-bootstrap design score and an oracle upper bound that uses oracle feasibility directly to verify metric well-formedness. The pseudo-bootstrap score is a non-neural sanity-check rule used only to verify that the evaluation pipeline separates curve reconstruction from feasible-candidate retrieval; it is not used to support any claim about surrogate superiority.

Cross-material transfer

For cross-material transfer, each per-material checkpoint is evaluated on every other material’s held-out pool. Only the dimensionless scaling and material vector m^* are swapped to those of the target card; no retraining or fine-tuning is performed. The transfer matrix thus isolates the inductive bias the network absorbed during training from the dimensional-scale change that the Buckingham- π formulation neutralises. All transfer numbers in the manuscript are reported under PINN-energy unless noted; the supplementary material includes the equivalent matrices for MLP-softplus and PINN-full.

Reporting and reproducibility

The manuscript reports model architecture, input representation, training data generation, random seeds, optimisation settings, checkpoint metadata, evaluation metrics and baseline comparisons to support reproducibility. The candidate pools, oracle labels, dimensionless inputs, training hyperparameters, optimiser state, checkpoint hashes, evaluation scripts and machine-readable metric tables are bundled in the repository together with this manuscript. The supplementary material provides full per-method, per-material and per-transfer tables that underline the compact summaries in the main text.

Data availability

The numerical benchmark archive, including candidate pools, generated metrics, figures, configuration files and run metadata, is available in the project repository at <https://github.com/Dyniel/pinn-gym>.

Code availability

The code is available at <https://github.com/Dyniel/pinn-gym>. The repository contains scripts for candidate generation, oracle evaluation, model training, metric aggregation and figure reproduction.

Acknowledgements

The authors received no specific funding for this work.

Author contributions

D.C. conceived the benchmark framing, implemented and curated the numerical workflow, analysed the results, prepared the figures and tables, and wrote the manuscript. A.C. supervised the research direction, provided conceptual guidance, and reviewed the manuscript.

Competing interests

The authors declare no competing interests.

Use of generative AI in manuscript preparation

Generative AI assistants were used for language polishing and to suggest restructuring of paragraphs in the introduction and discussion. All scientific content, methodology, code, oracle definitions, surrogate training, evaluation procedures, numerical results and interpretation are the authors' own. No generative AI was used to produce results, data, figures or citations; all citations were verified against the primary sources before inclusion.

References

1. Raissi, M., Perdikaris, P. & Karniadakis, G. E. Physics-informed neural networks: A deep learning framework for solving forward and inverse problems involving nonlinear partial differential equations. *J. Comput. Phys.* **378**, 686–707 (2019).
2. Karniadakis, G. E. *et al.* Physics-informed machine learning. *Nat. Rev. Phys.* **3**, 422–440 (2021).
3. Cuomo, S., Schiano di Cola, V., Giampaolo, F., Rozza, G., Raissi, M. & Piccialli, F. Scientific machine learning through physics-informed neural networks: Where we are and what's next. *J. Sci. Comput.* **92**, 88 (2022).
4. Wang, S., Sankaran, S., Wang, H. & Perdikaris, P. An expert's guide to training physics-informed neural networks. *arXiv preprint arXiv:2308.08468* (2023).
5. Toscano, J. D., Oommen, V., Varghese, A. J., Zou, Z., Daryakenari, N. A., Wu, C. & Karniadakis, G. E. From PINNs to PIKANs: recent advances in physics-informed machine learning. *arXiv preprint arXiv:2410.13228* (2024).
6. Gibson, L. J. & Ashby, M. F. *Cellular Solids: Structure and Properties*, 2nd edn. Cambridge University Press (1997).
7. Ashby, M. F. The properties of foams and lattices. *Philos. Trans. R. Soc. A* **364**, 15–30 (2006).
8. Bertoldi, K., Vitelli, V., Christensen, J. & van Hecke, M. Flexible mechanical metamaterials. *Nat. Rev. Mater.* **2**, 17066 (2017).
9. Liu, R. *et al.* A review on factors affecting the mechanical properties of additively manufactured lattice structures. *J. Mater. Eng. Perform.* **33**, 1–25 (2024).
10. Gu, G. X., Chen, C.-T., Richmond, D. J. & Buehler, M. J. Bioinspired hierarchical composite design using machine learning: simulation, additive manufacturing, and experiment. *Mater. Horiz.* **5**, 939–945 (2018).
11. Zheng, X., Zhang, X., Chen, T.-T. & Watanabe, I. Deep learning in mechanical metamaterials: from prediction and generation to inverse design. *Adv. Mater.* **35**, 2302530 (2023).
12. Maurizi, M., Gao, C. & Berto, F. Predicting stress, strain and deformation fields in materials and structures with graph neural networks. *Sci. Reports* **12**, 21834 (2022).

13. Buckingham, E. On physically similar systems; illustrations of the use of dimensional equations. *Phys. Rev.* **4**, 345–376 (1914).
14. Barenblatt, G. I. *Scaling, Self-similarity, and Intermediate Asymptotics*. Cambridge University Press (1996).
15. Takamoto, M., Praditia, T., Leiteritz, R., MacKinlay, D., Alesiani, F., Pflüger, D. & Niepert, M. PDEBench: An extensive benchmark for scientific machine learning. In *Advances in Neural Information Processing Systems* **35** (NeurIPS 2022).
16. Lu, L., Meng, X., Cai, S., Mao, Z., Goswami, S., Zhang, Z. & Karniadakis, G. E. A comprehensive and fair comparison of two neural operators (with practical extensions) based on FAIR data. *Comput. Methods Appl. Mech. Eng.* **393**, 114778 (2022).
17. Subramanian, S., Harrington, P., Keutzer, K., Bhimji, W., Morozov, D., Mahoney, M. W. & Gholami, A. Towards foundation models for scientific machine learning: characterizing scaling and transfer behavior. In *Advances in Neural Information Processing Systems* **36** (NeurIPS 2023).
18. Wang, S., Yu, X. & Perdikaris, P. When and why PINNs fail to train: a neural tangent kernel perspective. *J. Comput. Phys.* **449**, 110768 (2022).
19. Wang, S., Sankaran, S. & Perdikaris, P. Respecting causality is all you need for training physics-informed neural networks. *arXiv preprint arXiv:2203.07404* (2022).
20. Krishnapriyan, A. S., Gholami, A., Zhe, S., Kirby, R. & Mahoney, M. W. Characterizing possible failure modes in physics-informed neural networks. In *Advances in Neural Information Processing Systems* **34** (NeurIPS 2021).
21. Daw, A., Bu, J., Wang, S., Perdikaris, P. & Karpatne, A. Mitigating propagation failures in physics-informed neural networks using Retain-Resample-Release (R3) sampling. In *Proceedings of the 40th International Conference on Machine Learning (ICML 2023)*.
22. Bischof, R. & Kraus, M. A. Multi-objective loss balancing for physics-informed deep learning. *arXiv preprint arXiv:2110.09813* (2021).
23. Lu, L., Jin, P., Pang, G., Zhang, Z. & Karniadakis, G. E. Learning nonlinear operators via DeepONet based on the universal approximation theorem of operators. *Nat. Mach. Intell.* **3**, 218–229 (2021).
24. Li, Z., Kovachki, N. B., Azizzadenesheli, K., Liu, B., Bhattacharya, K., Stuart, A. & Anandkumar, A. Fourier neural operator for parametric partial differential equations. In *International Conference on Learning Representations (ICLR 2021)*.
25. Kovachki, N. B., Li, Z., Liu, B., Azizzadenesheli, K., Bhattacharya, K., Stuart, A. & Anandkumar, A. Neural operator: learning maps between function spaces with applications to PDEs. *J. Mach. Learn. Res.* **24**, 1–97 (2023).
26. Psaros, A. F., Meng, X., Zou, Z., Guo, L. & Karniadakis, G. E. Uncertainty quantification in scientific machine learning: methods, metrics, and comparisons. *J. Comput. Phys.* **477**, 111902 (2023).
27. Zou, Z., Meng, X., Psaros, A. F. & Karniadakis, G. E. NeuralUQ: a comprehensive library for uncertainty quantification in neural differential equations and operators. *SIAM Rev.* **66**, 161–190 (2024).